reagents, materials and analysis tools; Y.K., Y.O., Y.S., M.N., K.Y., S.Y., S.S., T.A., R.H., and S.U. recruited the patients; R.T., H.M., and S.Y. provided critical reading and scientific discussions; T.S., K.K., T.T., and K. Takahashi performed microarray analysis; T.A. performed karyotyping; A.W. performed bisulfite genomic sequencing; K.I. and D.W. performed electrophysiology; K. Tsukita, T.K., and H.H. produced the lentivirus; H.I., N.I., M.A., and T.K. wrote the paper. The experimental protocols dealing with human or animal subjects were approved by the institutional review board at each institute. S.Y. is a member without salary of the scientific advisory boards of iPierian, iPS Academia Japan, Megakaryon Corporation, and Retina Institute Japan.

Received: February 27, 2012
Revised: December 22, 2012
Accepted: January 18, 2013
Published: February 21, 2013

REFERENCES

Barnham, K.J., Masters, C.L., and Bush, A.I. (2004). Neurodegenerative diseases and oxidative stress. Nat. Rev. Drug Discov. *3*, 205–214.

Begum, G., Kintner, D., Liu, Y., Cramer, S.W., and Sun, D. (2012). DHA inhibits ER Ca^{2+} release and ER stress in astrocytes following in vitro ischemia. J. Neurochem. *120*, 622–630.

Butterfield, D.A. (2003). Amyloid β-peptide [1-42]-associated free radical-induced oxidative stress and neurodegeneration in Alzheimer's disease brain: mechanisms and consequences. Curr. Med. Chem. *10*, 2651–2659.

Cole, G.M., and Frautschy, S.A. (2006). Docosahexaenoic acid protects from amyloid and dendritic pathology in an Alzheimer's disease mouse model. Nutr. Health *18*, 249–259.

Freund-Levi, Y., Eriksdotter-Jönhagen, M., Cederholm, T., Basun, H., Faxén-Irving, G., Garlind, A., Vedin, I., Vessby, B., Wahlund, L.O., and Palmblad, J. (2006). Omega-3 fatty acid treatment in 174 patients with mild to moderate Alzheimer disease: OmegAD study: a randomized double-blind trial. Arch. Neurol. *63*, 1402–1408.

Gong, Y., Chang, L., Viola, K.L., Lacor, P.N., Lambert, M.P., Finch, C.E., Krafft, G.A., and Klein, W.L. (2003). Alzheimer's disease-affected brain: presence of oligomeric A β ligands (ADDLs) suggests a molecular basis for reversible memory loss. Proc. Natl. Acad. Sci. USA *100*, 10417–10422.

Haass, C., and Selkoe, D.J. (2007). Soluble protein oligomers in neurodegeneration: lessons from the Alzheimer's amyloid β-peptide. Nat. Rev. Mol. Cell Biol. *8*, 101–112.

Hensley, K., Carney, J.M., Mattson, M.P., Aksenova, M., Harris, M., Wu, J.F., Floyd, R.A., and Butterfield, D.A. (1994). A model for β-amyloid aggregation and neurotoxicity based on free radical generation by the peptide: relevance to Alzheimer disease. Proc. Natl. Acad. Sci. USA *91*, 3270–3274.

Israel, M.A., Yuan, S.H., Bardy, C., Reyna, S.M., Mu, Y., Herrera, C., Hefferan, M.P., Van Gorp, S., Nazor, K.L., Boscolo, F.S., et al. (2012). Probing sporadic and familial Alzheimer's disease using induced pluripotent stem cells. Nature *482*, 216–220.

Kassler, K., Horn, A.H., and Sticht, H. (2010). Effect of pathogenic mutations on the structure and dynamics of Alzheimer's A β 42-amyloid oligomers. J. Mol. Model. *16*, 1011–1020.

Krafft, G.A., and Klein, W.L. (2010). ADDLs and the signaling web that leads to Alzheimer's disease. Neuropharmacology *59*, 230–242.

Krencik, R., Weick, J.P., Liu, Y., Zhang, Z.J., and Zhang, S.C. (2011). Specification of transplantable astroglial subtypes from human pluripotent stem cells. Nat. Biotechnol. *29*, 528–534.

Kuo, Y.M., Emmerling, M.R., Vigo-Pelfrey, C., Kasunic, T.C., Kirkpatrick, J.B., Murdoch, G.H., Ball, M.J., and Roher, A.E. (1996). Water-soluble Abeta (N-40, N-42) oligomers in normal and Alzheimer disease brains. J. Biol. Chem. *271*, 4077–4081.

Lambert, M.P., Velasco, P.T., Chang, L., Viola, K.L., Fernandez, S., Lacor, P.N., Khuon, D., Gong, Y., Bigio, E.H., Shaw, P., et al. (2007). Monoclonal antibodies that target pathological assemblies of Abeta. J. Neurochem. *100*, 23–35.

Lee, M., You, H.J., Cho, S.H., Woo, C.H., Yoo, M.H., Joe, E.H., and Kim, J.H. (2002). Implication of the small GTPase Rac1 in the generation of reactive oxygen species in response to β-amyloid in C6 astroglioma cells. Biochem. J. *366*, 937–943.

Lesné, S., Koh, M.T., Kotilinek, L., Kayed, R., Glabe, C.G., Yang, A., Gallagher, M., and Ashe, K.H. (2006). A specific amyloid-β protein assembly in the brain impairs memory. Nature *440*, 352–357.

Malhotra, J.D., and Kaufman, R.J. (2007). Endoplasmic reticulum stress and oxidative stress: a vicious cycle or a double-edged sword? Antioxid. Redox Signal. *9*, 2277–2293.

Morizane, A., Doi, D., Kikuchi, T., Nishimura, K., and Takahashi, J. (2011). Small-molecule inhibitors of bone morphogenic protein and activin/nodal signals promote highly efficient neural induction from human pluripotent stem cells. J. Neurosci. Res. *89*, 117–126.

Murakami, K., Horikoshi-Sakuraba, Y., Murata, N., Noda, Y., Masuda, Y., Kinoshita, N., Hatsuta, H., Murayama, S., Shirasawa, T., Shimizu, T., and Irie, K. (2010). Monoclonal antibody against the turn of the 42-residue amyloid β-protein at positions 22 and 23. ACS Chem. Neurosci. *1*, 747–756.

Nishitsuji, K., Tomiyama, T., Ishibashi, K., Ito, K., Teraoka, R., Lambert, M.P., Klein, W.L., and Mori, H. (2009). The E693Δ mutation in amyloid precursor protein increases intracellular accumulation of amyloid β oligomers and causes endoplasmic reticulum stress-induced apoptosis in cultured cells. Am. J. Pathol. *174*, 957–969.

Noguchi, A., Matsumura, S., Dezawa, M., Tada, M., Yanazawa, M., Ito, A., Akioka, M., Kikuchi, S., Sato, M., Ideno, S., et al. (2009). Isolation and characterization of patient-derived, toxic, high mass amyloid β-protein (Abeta) assembly from Alzheimer disease brains. J. Biol. Chem. *284*, 32895–32905.

Okita, K., Matsumura, Y., Sato, Y., Okada, A., Morizane, A., Okamoto, S., Hong, H., Nakagawa, M., Tanabe, K., Tezuka, K., et al. (2011). A more efficient method to generate integration-free human iPS cells. Nat. Methods *8*, 409–412.

Quinn, J.F., Raman, R., Thomas, R.G., Yurko-Mauro, K., Nelson, E.B., Van Dyck, C., Galvin, J.E., Emond, J., Jack, C.R., Jr., Weiner, M., et al. (2010). Docosahexaenoic acid supplementation and cognitive decline in Alzheimer disease: a randomized trial. JAMA *304*, 1903–1911.

Shankar, G.M., Li, S., Mehta, T.H., Garcia-Munoz, A., Shepardson, N.E., Smith, I., Brett, F.M., Farrell, M.A., Rowan, M.J., Lemere, C.A., et al. (2008). Amyloid-β protein dimers isolated directly from Alzheimer's brains impair synaptic plasticity and memory. Nat. Med. *14*, 837–842.

Shimada, H., Ataka, S., Tomiyama, T., Takechi, H., Mori, H., and Miki, T. (2011). Clinical course of patients with familial early-onset Alzheimer's disease potentially lacking senile plaques bearing the E693Δ mutation in amyloid precursor protein. Dement. Geriatr. Cogn. Disord. *32*, 45–54.

Takano, K., Kitao, Y., Tabata, Y., Miura, H., Sato, K., Takuma, K., Yamada, K., Hibino, S., Choshi, T., Iinuma, M., et al. (2007). A dibenzoylmethane derivative protects dopaminergic neurons against both oxidative stress and endoplasmic reticulum stress. Am. J. Physiol. Cell Physiol. *293*, C1884–C1894.

Tomiyama, T., Nagata, T., Shimada, H., Teraoka, R., Fukushima, A., Kanemitsu, H., Takuma, H., Kuwano, R., Imagawa, M., Ataka, S., et al. (2008). A new amyloid β variant favoring oligomerization in Alzheimer's-type dementia. Ann. Neurol. *63*, 377–387.

Tomiyama, T., Matsuyama, S., Iso, H., Umeda, T., Takuma, H., Ohnishi, K., Ishibashi, K., Teraoka, R., Sakama, N., Yamashita, T., et al. (2010). A mouse model of amyloid β oligomers: their contribution to synaptic alteration, abnormal tau phosphorylation, glial activation, and neuronal loss *in vivo*. J. Neurosci. *30*, 4845–4856.

Walsh, D.M., Klyubin, I., Fadeeva, J.V., Cullen, W.K., Anwyl, R., Wolfe, M.S., Rowan, M.J., and Selkoe, D.J. (2002). Naturally secreted oligomers of amyloid β protein potently inhibit hippocampal long-term potentiation *in vivo*. Nature *416*, 535–539.

Yagi, T., Ito, D., Okada, Y., Akamatsu, W., Nihei, Y., Yoshizaki, T., Yamanaka, S., Okano, H., and Suzuki, N. (2011). Modeling familial Alzheimer's disease with induced pluripotent stem cells. Hum. Mol. Genet. *20*, 4530–4539.

The American Journal of Pathology, Vol. 183, No. 1, July 2013

ELSEVIER

The American Journal of
PATHOLOGY

ajp.amjpathol.org

MOLECULAR PATHOGENESIS OF GENETIC AND INHERITED DISEASES

Neurodegenerative Disorder FTDP-17—Related Tau Intron 10 +16C→T Mutation Increases Tau Exon 10 Splicing and Causes Tauopathy in Transgenic Mice

Tomohiro Umeda,*† Takenari Yamashita,* Tetsuya Kimura,‡ Kiyouhisa Ohnishi,* Hiroshi Takuma,* Tomoko Ozeki,§ Akihiko Takashima,‡ Takami Tomiyama,*† and Hiroshi Mori*†

From the Department of Neuroscience, Osaka City University Graduate School of Medicine, Osaka; Core Research for Evolutional Science and Technology,† Japan Science and Technology Agency, Saitama; the Department of Aging Neurobiology,‡ Center for Development of Advanced Medicine for Dementia, National Center for Geriatrics and Gerontology, Obu; and the School of Comprehensive Rehabilitation,§ Osaka Prefecture University, Sakai, Japan*

Accepted for publication March 21, 2013.

Address correspondence to Hiroshi Mori, Ph.D., Department of Neuroscience, Osaka City University Graduate School of Medicine, 1-4-3 Asahimachi, Abeno-ku, Osaka 545-8585, Japan. E-mail: mori@med.osaka-cu.ac.jp.

Frontotemporal dementia and parkinsonism linked to chromosome 17 (FTDP-17) is a neurodegenerative disorder caused by mutations in the tau gene. Many mutations identified in FTDP-17 have been shown to affect tau exon 10 splicing *in vitro*, which presumably causes pathologic imbalances in exon 10^- [3-repeat (3R)] and exon 10^+ [4-repeat (4R)] tau expression and leads to intracellular inclusions of hyperphosphorylated tau in patient brains. However, no reports have investigated this theory using model mice with a tau intronic mutation. Herein, we generated new transgenic mice harboring the tau intron 10 +16C→T mutation. We prepared a transgene construct containing intronic sequences required for exon 10 splicing in the longest tau isoform cDNA. Although mice bearing the construct without the intronic mutation showed normal developmental changes of the tau isoform from 3R tau to equal amounts of 3R and 4R tau, mice with the mutation showed much higher levels of 4R tau at the adult stage. 4R tau was selectively recovered in insoluble brain fractions in their old age. Furthermore, these mice displayed abnormal tau phosphorylation, synapse loss and dysfunction, memory impairment, glial activation, tangle formation, and neuronal loss in an age-dependent manner. These findings provide the first evidence in a mouse model that a tau intronic mutation—induced imbalance of 3R and 4R tau could be a cause of tauopathy. *(Am J Pathol 2013, 183: 211—225; http://dx.doi.org/10.1016/j.ajpath.2013.03.015)*

Frontotemporal dementia and parkinsonism linked to chromosome 17 (FTDP-17) is a neurodegenerative disorder caused by mutations in the tau gene.[1] Its pathologic features include intracellular inclusions of hyperphosphorylated tau aggregates and frontotemporal lobar atrophy. Such tau inclusions are observed not only in FTDP-17 but also in many other neurodegenerative diseases, including Alzheimer disease, which are collectively called tauopathy.[2]

Tau is an axonal microtubule-associated protein and contributes to microtubule stabilization. There are six tau isoforms in humans, the result of alternative splicing of exons 2, 3, and 10 from a single gene. Exon 10 encodes the second of four microtubule-binding domains (MBDs). The alternative splicing of exon 10 generates two types of tau isoforms: exon 10^- mRNA produces 3-repeat (3R) tau with three MBDs, and exon 10^+ mRNA produces 4-repeat (4R) tau with four MBDs. Tau mutations have been identified in exons and introns. Exonic mutations are largely located in or near MBDs and have been shown to attenuate the ability of tau to bind to microtubules,[3,4] enhance tau self-aggregation,[5] and affect exon 10 splicing.[6] All but one intronic mutation is located in the 5′ region of intron 10 and has been shown to affect exon 10 splicing.[7,8] It is known that tau exon 10 splicing is developmentally regulated; in fetal brains, 3R tau is exclusively

Supported by Grants-in-Aid for Scientific Research from the Ministry of Education, Culture, Sports, Science and Technology of Japan (21390271, 21500352, and 23110514); by Grants-in-Aid for Comprehensive Research on Dementia from the Ministry of Health, Labour, and Welfare of Japan; and, in part, by the Alzheimer's Association (IIRG-09-132098).

http://dx.doi.org/10.1016/j.ajpath.2013.03.015

expressed in rodents and humans; however, in adult brains, 4R tau expression becomes exclusive in rodents, whereas 3R and 4R tau are comparably expressed at a ratio of almost 1:1 in humans.[9–11] Thus, mutation-induced alteration of tau exon 10 splicing presumably causes pathologic imbalances in 3R and 4R tau, potentially leading to neurodegeneration. To date, many mouse models of FTDP-17 with tau missense mutations have been generated, but none include a tau intronic mutation.[12,13]

In the present study, we describe a new mouse model of FTDP-17 harboring a tau intron 10 +16C→T mutation and investigated its effects on exon 10 splicing and the onset of pathology *in vivo*. This mutation has been shown to increase tau exon 10 splicing *in vitro*[7,8,14] and cause an accumulation of 4R tau in insoluble fractions in patient brains.[15,16] Herein we show that the mutation indeed increased tau exon 10 splicing in adult mouse brains and subsequently caused abnormal tau phosphorylation, synapse loss and dysfunction, memory impairment, glial activation, tangle formation, and neuronal loss in an age-dependent manner. These findings provide the first evidence in a mouse model that an intronic mutation—induced imbalance in 3R and 4R tau could be a cause of tauopathy even in the absence of a missense sequence.

Materials and Methods

Antibodies

Rabbit polyclonal antibodies reactive to human and mouse tau (pool-2)[11] and specific to human tau (G2)[17] were prepared in our laboratory (Osaka City University Graduate School of Medicine, Osaka, Japan). Mouse monoclonal antibodies to tau phosphorylation at Ser396/Ser404 (PHF-1) and the conformational epitopes of pathologic tau (MC1) were gifts from Dr. Peter Davies (Department of Pathology, Albert Einstein College of Medicine, Bronx, NY). Mouse monoclonal antibodies to tau phosphorylation at Ser202/Thr205 (AT-8; Thermo Scientific, Waltham, MA), the presynaptic marker synaptophysin (SVP-38; Sigma-Aldrich, St. Louis, MO), the mature neuron marker NeuN (Chemicon International, Temecula, CA), the astrocyte marker glial fibrillary acidic protein (GFAP; Cappel, ICN Pharmaceuticals, Aurora, OH), and rabbit polyclonal antibodies to the microglia marker Iba-1 (Wako Pure Chemical Industries, Osaka, Japan) and actin (Sigma-Aldrich) were purchased.

Generation of Transgenic Mice

The transgene for generating transgenic (Tg) mice was prepared from a previously described human tau genomic construct.[18] This construct, tau iEi10, contains the first 18 nucleotides and the last 3.0 kb of tau intron 9 and the first 3.0 kb and the last 38 nucleotides of intron 10 at the corresponding sides of exon 10 in tau441 (the longest tau isoform) cDNA. The intron 10 +16C→T mutation was introduced by site-directed mutagenesis. After the SfiI site in the intron 10 sequence was destroyed by site-directed mutagenesis, tau iEi10 sequences with or without the intronic mutation were ligated into the EcoRV site of the pNN265 vector that contains a 5′ intron and a 3′ intron plus a poly A signal from SV40. This expression carriage was excised from pNN265 with NotI and was inserted into the NotI site of the pMM403 vector that contains the mouse 8.6-kb calcium/calmodulin-dependent kinase IIα promoter to make forebrain-specific transgene expression.[19] Calcium/calmodulin-dependent kinase IIα—tau iEi10 linear sequences were excised from pMM403 with SfiI and injected into B6C3F1 mouse embryos. The obtained Tg mice were backcrossed with C57BL/6 mice for at least 10 generations. All the mice used were heterozygous for the transgene of interest. Expression levels of human tau were determined by Western blot analysis with G2 and pool-2 antibodies. All the animal experiments were approved by the ethics committee of Osaka City University (Osaka, Japan) and were performed in accordance with the Guide for Animal Experimentation, Osaka City University. Every effort was made to minimize the number of animals used and their suffering. The ages and numbers of Tg mice subjected to each assay are summarized in Table 1.

RT-PCR

To examine tau exon 10 splicing in Tg mice, RT-PCR was performed between tau exons 9 and 11. RNA was isolated from brain tissues of the intronic mutant and control Tg mice as well as non-Tg littermates at 7 days and 4 months of age using the SV total RNA isolation kit (Promega, Madison, WI). Reverse transcription and PCR were performed essentially as described previously[7] to separately amplify endogenous mouse tau and transgene-derived human tau. Primer sequences used were as follows: mouse exon 9F, 5′-CACCAAAATCCGGAGAACGA-3′; mouse exon 11R, 5′-CTTTGCTCAGGTCCACCGGC-3′; human exon 9F, 5′-CTCCAAAATCAGGGGATCGC-3′; and human exon 11R, 5′-CCTTGCTCAGGTCAACTGGT-3′. PCR was performed as 30 cycles at 94°C for 30 seconds, at 62°C for 30 seconds, and at 72°C for 45 seconds, with a final 72°C extension for 10 minutes. The expected sizes of PCR products were 390 bp for exon 10^+ mRNA and 297 bp for exon 10^- mRNA for mouse and human tau.

Western Blot Analysis

Mouse brains, not including the hindbrain, were homogenized by sonication in four volumes of 100 mmol/L Tris-HCl, pH 7.6, and 150 mmol/L NaCl Tris-buffered saline (TBS) containing protease inhibitor cocktail (P8340; Sigma-Aldrich). The homogenates were fractionated by three-step ultracentrifugation, including TBS, N-lauroylsarcosinate (sarkosyl), and guanidine hydrochloride (GuHCl) extraction, essentially as described previously.[20] In brief, the homogenates were centrifuged at 100,000 × *g* at 4°C for 15 minutes, and the supernatants were harvested as the TBS-soluble fractions. The

precipitates were dissolved by sonication in four volumes of tissue weight of 1% sarkosyl/TBS containing P8340 and then were incubated for 1 hour at room temperature. After centrifugation at 100,000 × *g* at room temperature for 15 minutes, the supernatants were removed. The sarkosyl-insoluble precipitates were then dissolved by sonication in two volumes of tissue weight of 4 mol/L GuHCl and incubated for 1 hour at room temperature. After a second centrifugation, the supernatants were harvested and their solvent (GuHCl) was exchanged with TBS containing P8340 using Amicon Ultra 10K filter devices (Millipore, Billerica, MA). For dephosphorylation of tau, 50 μL of the TBS- and GuHCl-soluble (sarkosyl-insoluble) fractions were treated with 400 U/mL of calf intestinal alkaline phosphatase (New England Biolabs, Ipswich, MA) at 37°C for 16 hours in the presence of 10 mmol/L $MgCl_2$ and 1 mmol/L dithiothreitol. The samples were subjected to SDS-PAGE with 7% NuPAGE Tris-acetate gels (Invitrogen, Carlsbad, CA) and were transferred to polyvinylidene difluoride membranes (Millipore). Tau was probed with pool-2 or G2 antibody followed by horseradish peroxidase–labeled second antibody and the chemiluminescent substrate Immobilon Western (Millipore). As a loading control, actin in TBS-soluble fractions was also probed with a corresponding antibody. Signals were visualized and quantified using a LAS-3000 luminescent image analyzer (Fujifilm, Tokyo, Japan).

IHC Analysis and Silver Staining

Tg mice and non-Tg littermates were examined for tau phosphorylation, synapse loss, glial activation, and neuronal loss at 2, 4, 6, 8, 12, 18, and 24 months of age by immunohistochemical (IHC) analysis and for tangle formation at 18 and 24 months of age by silver staining. Mouse brains were fixed in 4% paraformaldehyde, embedded in paraffin, sectioned at 5 μm, and deparaffinized with xylene and ethanol. For only tau staining, the sections were pretreated by boiling in 0.01 N HCl (pH 2) for 10 minutes to expose the epitopes. As we previously reported,[21] the pretreatment of sections enhanced GFAP and Iba-1 staining, but such an enhancement made the difference between mutant Tg mice and control mice unclear. Thus, we used untreated sections in staining for these markers, which resulted in almost no intense staining in control mouse sections. IHC analysis was performed essentially as described previously.[21] Silver staining of the sections was performed according to the method of Gallyas.[22] Synapse loss was assessed by quantifying synaptophysin fluorescence intensity in the apical dendritic-somata field in the hippocampal CA3 region using ImageJ software version 1.45s (NIH, Bethesda, MD). Analysis was performed in a 30 × 60–μm area and in a larger, 110 × 110–μm area: the former includes the pyramidal cell layer (pcl) and the striatum lucidum (sl) close to the pcl (referred to as sl1), whereas the latter includes the pcl, sl1, and sl close to the stratum radiatum (sr) (referred to as sl2). Glial activation and neuronal loss were estimated by counting Iba-1-, GFAP-, and NeuN-positive cells in the following regions: Iba-1 in a 220 × 160–μm area in the hippocampal CA1 region, GFAP in a 220 × 160–μm area in the hippocampal CA2/3 region, and NeuN within 1000 μm along the pcl in the hippocampal CA1 region and in a 1 × 1–mm area in the retrosplenial region of the cerebral cortex.

Immunoelectron Microscopy

To examine tau filament formation, postembedding immunoelectron microscopy was performed in 24-month-old mutant Tg mice (line 609). Mouse brains were fixed in 4% paraformaldehyde and cut into 50-μm-thick sections using a vibratome. The sections were postfixed in 2.5% glutaraldehyde overnight, followed by 1% osmium tetroxide for 1.5 hours, dehydrated through a graded alcohol series, and embedded in epoxy resin. Then, ultrathin sections (70 nm thick) were prepared using an ultramicrotome. The sections were placed on H75-mesh carbon-coated copper grids, blocked with 5% bovine serum albumin/PBS for 10 minutes,

Table 1 Numbers of Tg Mice by Age Subjected to Each Assay and a Summary of the Results

		Ages (months)					
Figure No.	Assays	4	6	8	12	18	24
1	Tau WB	√ $n = 4$					
	Tau RT-PCR	√ $n = 4$					
2	Tau IHC	− $n = 5$	+ $n = 6$	+ $n = 4$	+ $n = 3$	+ $n = 4$	+ $n = 6$
3	Gallyas staining					− $n = 4$	+ $n = 6$
	Insoluble tau WB						+ $n = 2$
	ImmunoEM						+ $n = 3$
4	Synaptophysin IHC	− $n = 3$	+ $n = 3$	+ $n = 3$			+ $n = 4$
5	Electrophysiology		+ $n = 4$-5				
6	MWM	− $n = 6$-9	+ $n = 10$				
7	Iba1 IHC			− $n = 4$	+ $n = 4$	+ $n = 4$	+ $n = 4$
	GFAP IHC				− $n = 4$	− $n = 4$	+ $n = 4$
8	NeuN IHC					− $n = 4$	+ $n = 4$

√, done; −, pathology negative; +, pathology positive; EM, electron microscopy; MWM, Morris water maze; WB, Western blot analysis.

and incubated with pool-2 antibody for 1 hour, followed by 10 nm of gold particle–labeled second antibody (AuroProbe EM GAR G10; Amersham Biosciences, Piscataway, NJ) for 1 hour. The specimens were then stained with 2.5% lead citrate and 5% uranyl acetate and were viewed under an H-7500 electron microscope (Hitachi High-Technologies, Tokyo, Japan). Sarkosyl-insoluble brain fractions from 24-month-old mutant Tg mice (line 609) were also examined for tau filaments by immunoelectron microscopy. The supernatants of GuHCl-soluble (sarkosyl-insoluble) fractions prepared as described above were 100-fold diluted in TBS, sonicated for 1 minute, and absorbed onto 200-mesh carbon-coated nickel grids. The grids were blocked with 1% bovine serum albumin/PBS and were incubated with pool-2 antibody, followed by 10 nm of gold particle–labeled second antibody, as described above (see *Western Blot Analysis*). The specimens were negatively stained with 2% phosphotungstate and were viewed using an electron microscope.

Electrophysiologic Testing

Experiments were performed using 350-μm-thick transverse hippocampal slices obtained from 6-month-old male mutant Tg mice (line 609) and non-Tg littermates. Slices were prepared using a vibratome and were kept in an interface culture chamber at room temperature for ≥3 hours. In the recording chamber, the slices were perfused at a rate of 3 mL/min with artificial cerebrospinal fluid containing 125 mmol/L NaCl, 3.5 mmol/L KCl, 1.3 mmol/L $MgSO_4$, 1.2 mmol/L KH_2PO_4, 2.4 mmol/L $CaCl_2$, 26 mmol/L $NaHCO_3$, and 10 mmol/L glucose, bubbled with 95% O_2/5% CO_2, pH 7.4. Electrical stimulation (100-μsec pulse duration, 30- to 100-μA amplitude) was applied onto the middle point of the sl in the CA3 region using a bipolar tungsten electrode. Field excitatory postsynaptic potentials (fEPSPs) were recorded from four different areas of the apical dendritic-somata field in the CA3 region: the pcl close to the sl, the sl1, the sl2, and the sr close to the sl. Electrical response signals were 100-fold amplified using an ER-1 differential extracellular amplifier (Cygnus Technology, Delaware Water Gap, PA) and were recorded using a computer-assisted Digidata 1321A analog-to-digital converter (Axon Instruments, Union City, CA). The amplitude and slope of each fEPSP were analyzed using a custom-made application based on Matlab software, version 8 (The MathWorks Inc., Natick, MA). Input/output (I/O) curves were prepared in each area with increasing stimulus intensities. In long-term potentiation (LTP) measurement, we selected a recording point from the sl1/2 area in each slice, at the point which the maximum amplitude of fEPSP in the I/O curve was >1 mV. Stimulus intensity was set so that the basal level of fEPSP was 40% of the maximum amplitude. After baseline recording (30-second pulse interval) for 30 minutes, high-frequency stimulation (3 trains of 100 Hz/100 pulse bursts spaced 180 seconds apart) was delivered, and fEPSPs were subsequently recorded for 40 minutes.

Behavioral Tests

Spatial reference memory in mice was assessed at 4 and 6 months of age using the Morris water maze essentially as described previously.[21] Male mice were trained to swim to a hidden platform for 4 consecutive days, and the retention of spatial memory was assessed by a probe trial on day 5. Locomotor activities of the mice were examined by an open-field test as described previously.[21]

Statistical Analysis

All the data in the animal experiments are expressed as means ± SEM. Comparisons of means among more than two groups were performed using analysis of variance (for tau, synaptophysin, probe trial, Iba-1, GFAP, and NeuN) or two-factor repeated measures analysis of variance (for LTP and memory acquisition), followed by Fisher's protected least significant difference test. Comparison of I/O curves in electrophysiologic testing between two groups was performed using analysis of covariance. Differences with a $P < 0.05$ were considered significant.

Results

Generation of Tg Mice Harboring the Tau Intron 10 +16C→T Mutation

Tg mice expressing human wild-type tau in the presence or absence of the intron 10 +16C→T mutation were generated. The prepared transgenes contained the calcium/calmodulin-dependent kinase IIα promoter, human tau441 cDNA, and partial sequences of tau introns 9 and 10 inserted into the corresponding sides of exon 10 in tau cDNA (Figure 1A). Two lines of mutant Tg mice (lines 609 and 784) carrying the intronic mutation and one line of control Tg mice (line 264) having the same regions of introns 9 and 10 but not the mutation were established. Expression levels of total tau in brains at 4 months of age were determined by Western blot analysis with pool-2 antibody reactive to human and mouse tau (Figure 1B). Quantification of signals of the alkaline phosphatase–treated samples indicated that lines 264, 609, and 784 expressed tau protein at levels of 110%, 166%, and 186%, respectively, of those in non-Tg littermates (Figure 1C). This represents levels of human tau in these Tg mice of approximately 10%, 66%, and 86%, respectively, of the levels of endogenous mouse tau.

Increased Expression of 4R Tau in Intronic Mutant Mice

To examine the effect of the intronic mutation on exon 10 splicing, we measured the levels of tau exon 10^- and exon 10^+ mRNA in Tg mouse brains at 7 days and 4 months of age by RT-PCR (Figure 1D). For endogenous mouse tau, in control and mutant Tg mice, lines 264 and 609 expressed exon 10^- and exon 10^+ mRNA at a ratio of approximately

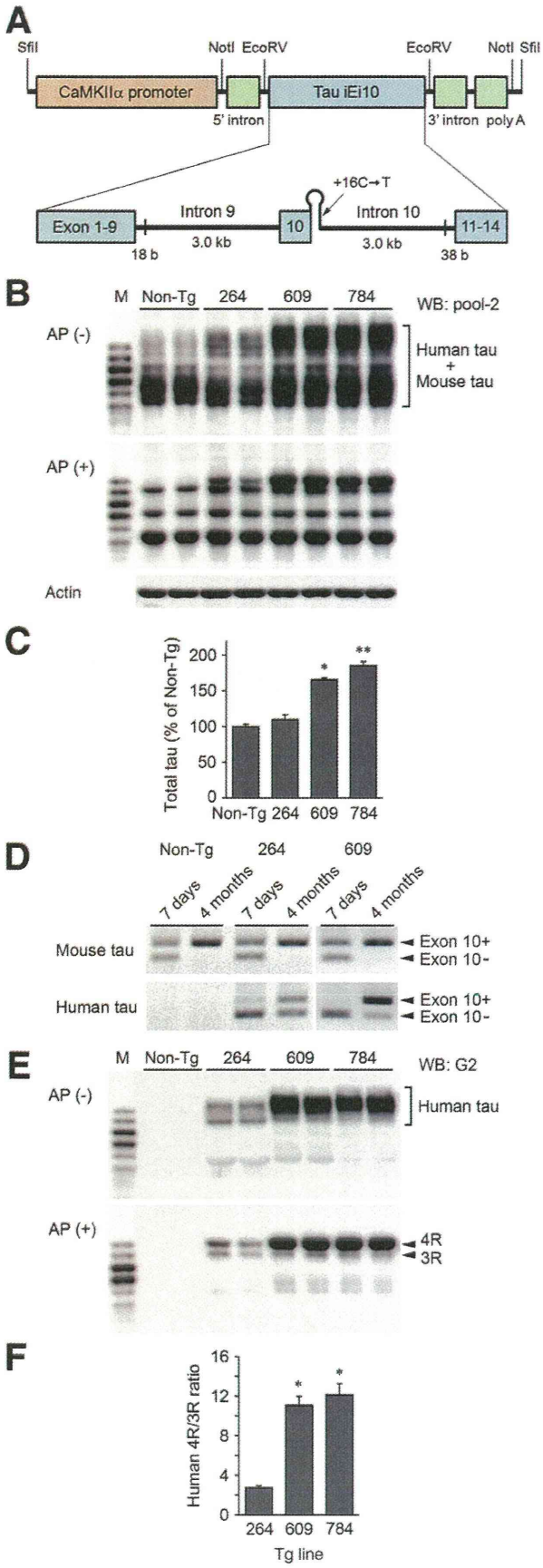

1:1 at 7 days of age but only exon 10^+ mRNA at 4 months of age. For transgene-derived human tau, lines 264 and 609 exclusively expressed exon 10^- mRNA at 7 days of age. At 4 months of age, however, line 264 expressed exon 10^- and exon 10^+ mRNA at a ratio of approximately 1:1, whereas line 609 predominantly expressed exon 10^+ mRNA. The latter was confirmed by Western blot analysis of 4-month-old brains with G2 antibody specific to human tau (Figure 1E). Quantification of signals of the alkaline phosphatase–treated samples revealed that line 264 expressed 3R and 4R human tau at comparable levels (the 4R/3R ratio was 2.7), whereas lines 609 and 784 predominantly expressed 4R human tau (the 4R/3R ratios were 11.1 and 12.1, respectively) (Figure 1F). These results indicate that control Tg mice possessed a developmental regulation of human tau exon 10 splicing that is similar to that in humans and that the mutant Tg mice reproduced an altered splicing of exon 10 to increase 4R tau expression at an adult age similar to that in patients with this mutation.

Abnormal Tau Phosphorylation and Tangle Formation in Intronic Mutant Mice

We next considered whether the altered splicing of tau exon 10 leads to tau pathologic abnormalities *in vivo*. Initially, we examined abnormal tau phosphorylation by IHC analysis with antibodies specific to phosphoepitopes of tau, AT-8 (Ser202/Thr205) (Figure 2, A–L) and PHF-1 (Ser396/Ser404) (Figure 2, M–O). Pathologic change of tau conformation was also examined with MC1 antibody (Figure 2, P–R). We confirmed that these antibodies did not react with brain sections from non-Tg littermates or line 264 even at 24 months of age (Figure 2, A–C). In contrast, lines 609 and 784 began to exhibit AT-8–, PHF-1–, and MC1-positive staining in hippocampal mossy fibers from

Figure 1 Generation of tau Tg mice with the intron 10 + 16C→T mutation. **A:** Transgene construct used to generate tau Tg mice. The tau DNA sequence came from the tau iEi10 construct that contains partial sequences of tau introns 9 and 10 at the corresponding sides of exon 10 in the longest tau isoform cDNA, allowing for alternative splicing of exon 10.[18] The predicted stem-loop structure in the 5′ splice site of exon 10 (splice donor site of intron 10) is shown. Two Tg lines (609 and 784) carrying the intron 10 + 16C→T mutation and one Tg line (264) without the mutation were established. CaMKIIα, calcium/calmodulin-dependent kinase IIα. **B:** Levels of expression of total tau in tau Tg mice. TBS-soluble fractions from brains of Tg mice and non-Tg littermates at 4 months of age were treated with or without alkaline phosphatase (AP) and were subjected to Western blot analysis (WB) with pool-2 antibody reactive to human and mouse tau. M, recombinant human tau 6 isoforms. **C:** Signal intensity of total tau in the AP-treated samples was quantified. $^*P < 0.0001$ versus non-Tg and line 264; $^{**}P < 0.0001$ versus non-Tg and line 264, $P = 0.0114$ versus line 609. **D:** Developmental change of tau exon 10 splicing in tau Tg mice. Tau exon 10 splicing was examined by RT-PCR between tau exons 9 and 11 using mouse tau and human tau specific primers. RNAs isolated from brains of Tg mice and non-Tg littermates at 7 days and 4 months of age were subjected to RT-PCR. **E:** Levels of expression of human tau in tau Tg mice. The same samples as in **B** were subjected to Western blot analysis with G2 antibody specific to human tau. **F:** Signal intensity of 3R and 4R tau in AP-treated samples was quantified, and the 4R/3R ratio was calculated. $^*P < 0.0001$ versus line 264. Data are given as means ± SEM ($n = 4$).

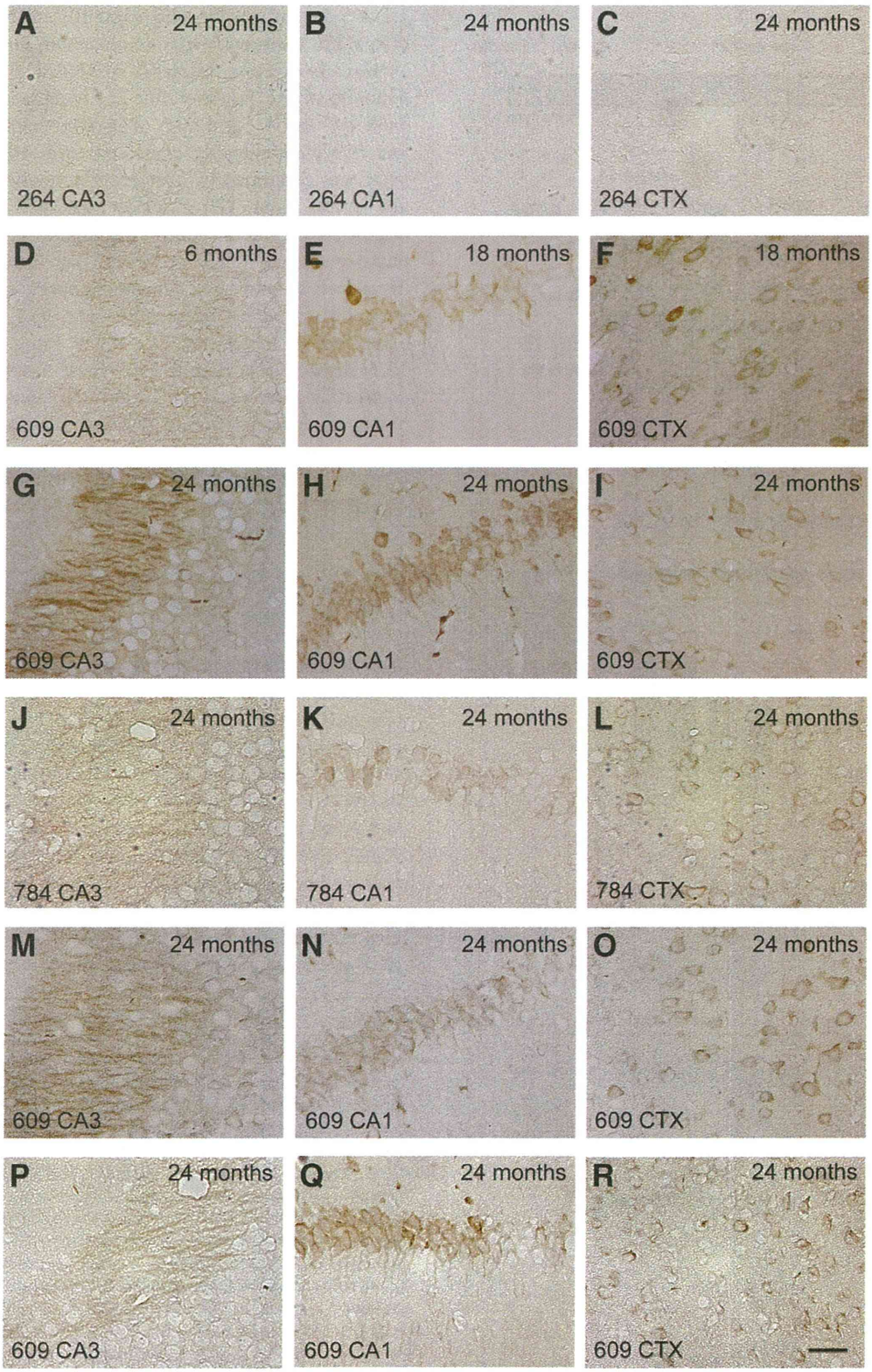

Figure 2 Abnormal tau phosphorylation in tau Tg mice. Brain sections from non-Tg littermates (data not shown), line 264 (**A**–**C**), line 609 (**D**–**I** and **M**–**R**), and line 784 (**J**–**L**) at various ages were stained with antibodies to phosphorylated tau, AT8 (**A**–**L**) and PHF-1 (**M**–**O**), and an antibody to pathologic conformation of tau, MC1 (**P**–**R**). Line 264 showed no positive staining even at 24 months of age (**A**–**C**). Lines 609 and 784 began to exhibit AT-8–, PHF-1–, and MC1-positive staining in hippocampal mossy fibers from 6 months of age (**D**) and in neuronal cell bodies of the hippocampus and cerebral cortex from 18 months of age (**E** and **F**). Images were taken from the CA3 (**A, D, G, J, M,** and **P**) and CA1 (**B, E, H, K, N,** and **Q**) regions of the hippocampus and from the retrosplenial region of the cerebral cortex (CTX; **C, F, I, L, O,** and **R**). Scale bar = 30 μm.

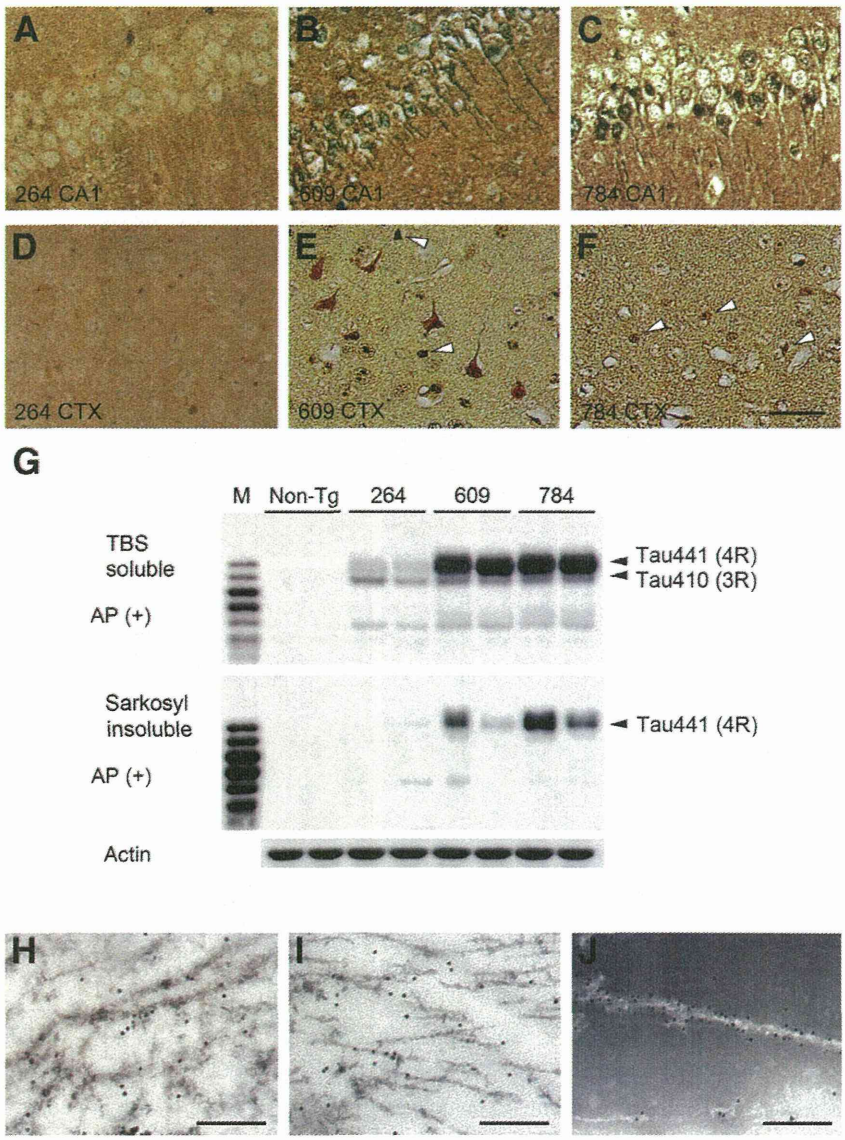

Figure 3 Tangles in tau Tg mice. **A**–**F**: Brain sections from Tg mice and non-Tg littermates at 18 and 24 months of age were stained by Gallyas silver staining. Line 264 showed no positive staining even at 24 months of age (**A** and **D**). Lines 609 (**B** and **E**) and 784 (**C** and **F**) displayed silver-positive inclusions in many neurons and glial cells (**arrowheads**) in the hippocampus and cerebral cortex at 24 months of age. Images were taken from the CA1 region (**A**–**C**) of the hippocampus and from the retrosplenial region of the cerebral cortex (CTX; **D**–**F**) at 24 months of age. **G**: Insoluble human tau in tau Tg mice. TBS-soluble and sarkosyl-insoluble fractions from brains at 24 months of age were treated with alkaline phosphatase (AP) and were subjected to Western blot analysis with G2 antibody. M, recombinant human tau 6 isoforms. **H**–**J**: Immunoelectron microscopy of tau filaments in tau Tg mice. Brain tissues from 24-month-old mutant tau Tg mice (line 609) were embedded in epoxy resin and cut into ultrathin sections (70 nm thick). The sections were incubated with pool-2 antibody followed by 10 nm of gold particle–labeled second antibody and then were stained with lead citrate and uranyl acetate. Images were taken from the CA1 region of the hippocampus (**H**) and from the retrosplenial region of the cerebral cortex (**I**). Sarkosyl-insoluble brain fractions from 24-month-old mutant tau Tg mice (line 609) were absorbed onto carbon-coated grids (**J**). The specimens were incubated with pool-2 antibody followed by 10 nm of gold particle–labeled second antibody and then were negatively stained. Scale bars: 30 μm (**A**–**F**); 200 nm (**H**–**J**).

6 months of age (Figure 2D) and in neuronal cell bodies of the hippocampus (particularly the CA1 region) and cerebral cortex (particularly the retrosplenial region) from 18 months of age (Figure 2, E and F).

The most characteristic tau pathologic abnormality in FTDP-17 is the formation of intracellular inclusions composed of hyperphosphorylated tau aggregates (so-called tangles). Thus, we examined whether these mutant Tg mice develop tangles at 18 and 24 months of age. We observed many neurons positively stained by Gallyas silver staining throughout the cell body in lines 609 and 784 at 24 months but not 18 months of age (Figure 3, A–F). Glial cells with positive staining were also detected at 24 months of age. These tangle-like inclusions were prominent in the CA1 region of the hippocampus and the retrosplenial region of the cerebral cortex. The intensities of the silver-positive staining in these mice, however, were weak compared with those in the brains of patients with Alzheimer disease (data not shown).

We further examined tau isoforms in insoluble brain fractions, as these are thought to be involved in tangle formation. Brain homogenates from 24-month-old mice were separated by three-step ultracentrifugation into TBS-, sarkosyl-, and GuHCl-soluble fractions. TBS- and GuHCl-soluble fractions were subjected to Western blot analysis with G2 antibody after dephosphorylation (Figure 3G). In the TBS-soluble fractions, we detected the same expression pattern of tau isoforms as observed at 4 months of age. In the sarkosyl-insoluble (GuHCl-soluble) fractions, however, lines 609 and 784, but not line 264, exhibited discrete bands for insoluble tau that corresponded to tau441, an isoform of 4R tau. These results are consistent with observations that 4R tau accumulates exclusively in sarkosyl-insoluble brain fractions from patients with this mutation.[15,16]

Tau inclusions are known to be composed of insoluble tau filaments. Thus, we examined tau filament formation in the brains of 24-month-old mutant Tg mice (line 609). In

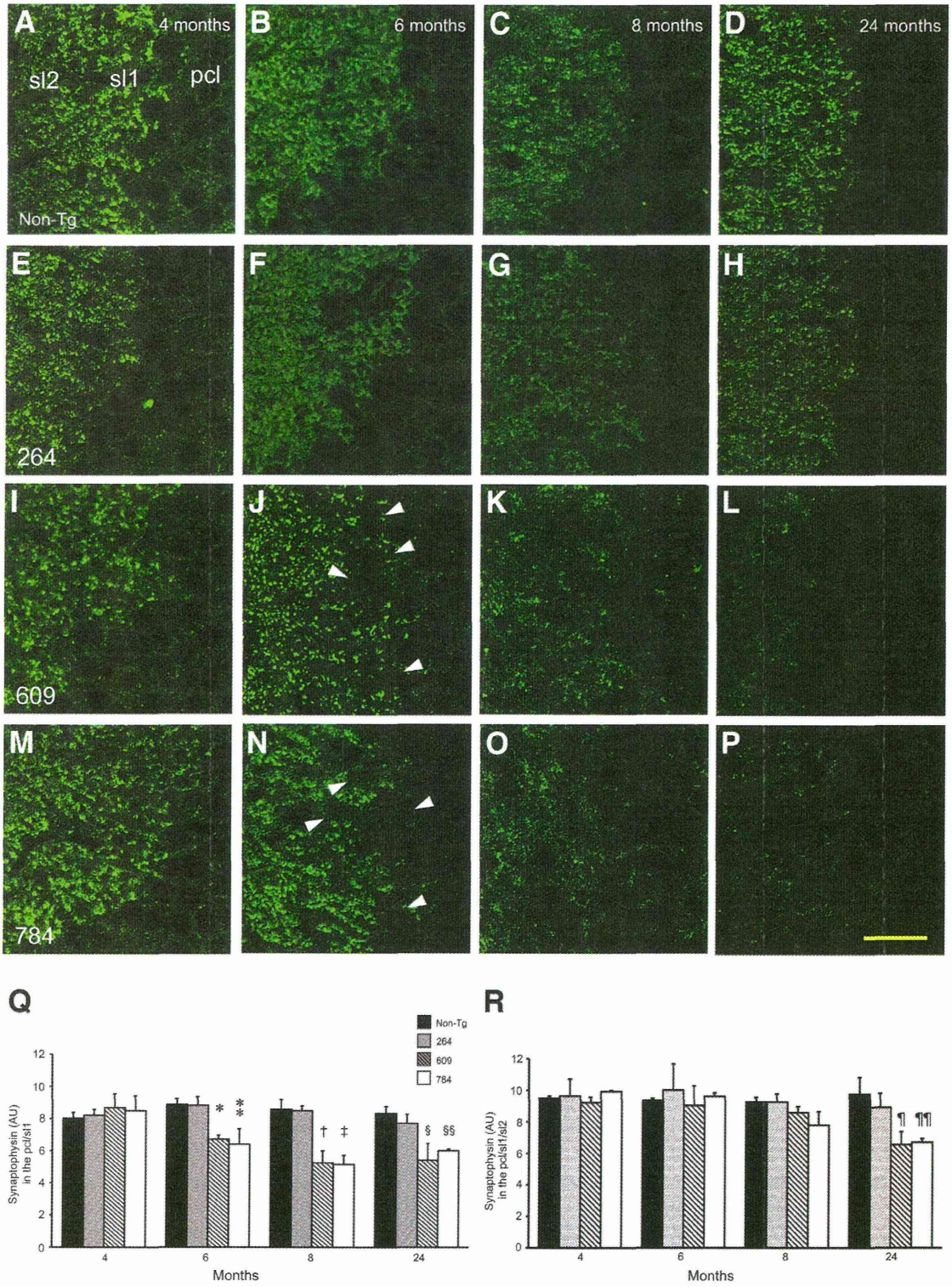

Figure 4 Age-dependent synapse loss in tau Tg mice. Brain sections from non-Tg littermates (**A**–**D**), line 264 (**E**–**H**), line 609 (**I**–**L**), and line 784 (**M**–**P**) at 4, 6, 8, and 24 months of age were stained with an antibody to the presynaptic marker synaptophysin. All the images were taken from the apical dendritic-somata field in the hippocampal CA3 region. Scare bar = 30 μm. Synaptophysin began to decrease from 6 months of age in the pcl/sl1 area in lines 609 and 784 (**arrowheads**). **Q** and **R**: Synaptophysin fluorescence intensity in the pcl/sl1 area (30 × 60 μm) (**Q**) and in the larger pcl/sl1/sl2 area (110 × 110 μm) (**R**) was quantified and is shown in arbitrary units (AU). Data are given as means ± SEM (n = 3 at 4 to 8 months, n = 4 at 24 months of age). *P = 0.0315 versus non-Tg, P = 0.0355 versus line 264; **P = 0.0173 versus non-Tg, P = 0.0194 versus line 264. †P = 0.0036 versus non-Tg, P = 0.0042 versus line 264. ‡P = 0.0031 versus non-Tg, P = 0.0035 versus line 264. §P = 0.0091 versus NonTg, P = 0.0298 versus 264; §§P = 0.0401 versus non-Tg. ¶P = 0.0222, ¶¶P = 0.0389 versus non-Tg.

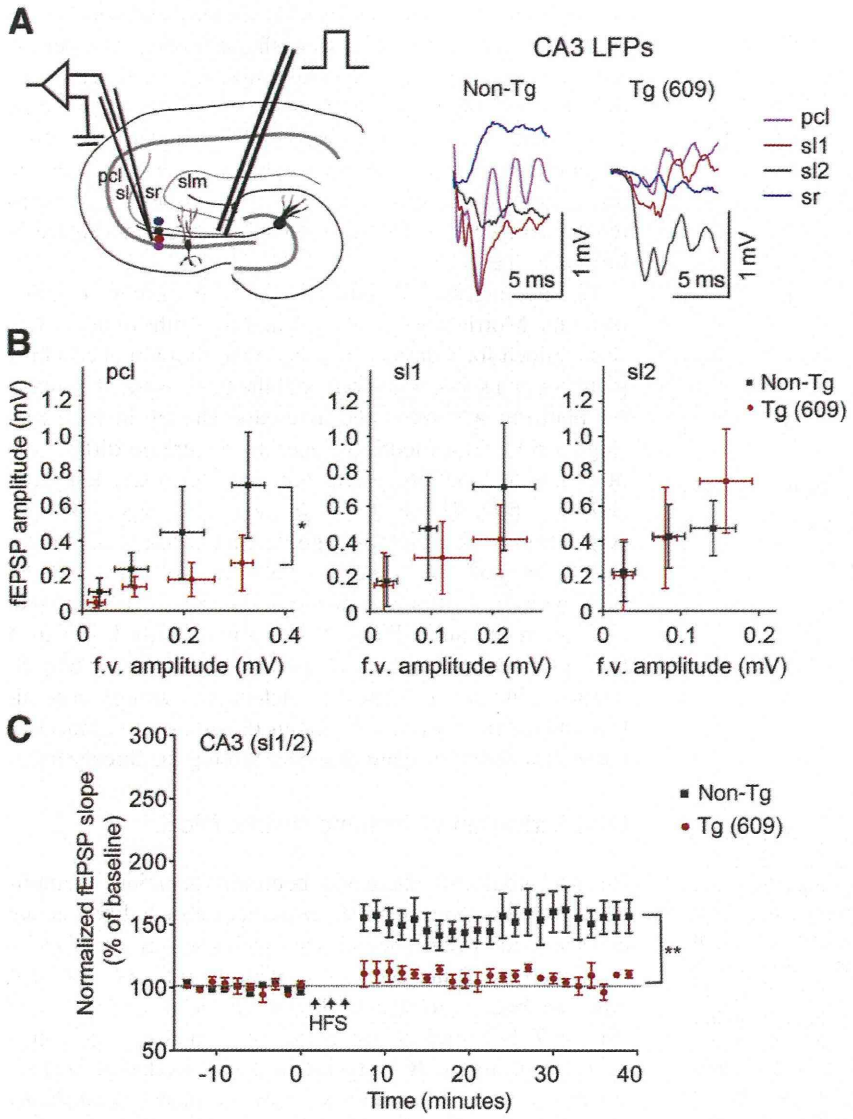

Figure 5 Synaptic dysfunction in tau Tg mice. Electrophysiologic testing was performed with hippocampal slices (350 μm thick) from 6-month-old male mutant Tg mice (line 609) and non-Tg littermates. **A:** Electrical stimulation was applied onto the middle point of the sl in the CA3 region, and evoked fEPSPs were recorded from four different areas of the apical dendritic-somata field in the CA3 region. Obtained local field potentials (LFPs) in these areas are shown. **B:** I/O curves were prepared in each area with increasing stimulus intensities. Magnitude of input is shown as fiber volley (f.v.) amplitude. $*P = 0.0003$ ($n = 4$; slices per group $n = 8$). **C:** LTP was measured from the sl1/2 area. High-frequency stimulation (HFS) stably induced LTP in non-Tg littermates but not in line 609. $**P = 0.0058$ ($n = 5$). Data are given as means ± SEM.

postembedding immunoelectron microscopy, we observed intracellular accumulation of pool-2–positive (ie, tau-positive) filamentous structures in the CA1 region of the hippocampus (Figure 3H) and the retrosplenial region of the cerebral cortex (Figure 3I). Sarkosyl-insoluble brain fractions from 24-month-old mutant Tg mice (line 609) were also examined for tau filaments. Immunoelectron microscopy revealed that these fractions contained abundant pool-2–positive filaments that appeared as a mixture of paired helical filament– and straight tubule–like structures (Figure 3J). Taken together, these results suggest that 4R tau overexpressed in mutant Tg mice assembled into insoluble filaments, which lead to tangle formation in the cell.

Synaptic and Cognitive Impairment in Intronic Mutant Mice

We next examined synaptic and cognitive impairments of Tg mice because the principal clinical symptom of FTDP-17 is dementia. Initially, synaptic density in the hippocampal CA3 region was evaluated by quantitative IHC analysis with an antibody to synaptophysin, a presynaptic marker protein (Figure 4, A–P). Non-Tg littermates and line 264 showed relatively constant and comparable levels of synaptic density at 4 months through 24 months of age in the pcl/sl1 area (Figure 4Q) and the larger psl/sl1/sl2 area (Figure 4R). On the other hand, lines 609 and 784 exhibited levels of synaptic density similar to non-Tg littermates at 4 months of age, but the levels began to decrease at 6 months of age in the pcl/sl1 area (Figure 4Q). However, when synaptophysin quantification was performed in the larger pcl/sl1/sl2 area, no significant differences were detected between non-Tg littermates and mutant Tg mice even at 8 months of age: the levels of synaptic density in this larger area in lines 609 and 784 significantly decreased later at 24 months of age (Figure 4R). We also performed Western blot analysis of synaptophysin levels in dissected whole hippocampal tissue, but again no significant differences between non-Tg littermates and